Geomechanics and Engineering, *Vol. 36, No. 5 (2024) 427-440*
https://doi.org/10.12989/gae.2024.36.5.427

Establishment of the roof model and optimization of the working face length in top coal caving mining

Chang-Xiang Wang[1], Qing-Heng Gu*[1,2], Meng Zhang[1], Cheng-Yang Jia[1], Bao-Liang Zhang[3] and Jian-Hang Wang[4]

[1]*State Key Laboratory of Mining Response and Disaster Prevention and Control in Deep Coal Mines Anhui University of Science and Technology, Huainan Anhui 232001,China*
[2]*State and Local Joint Engineering Laboratory for Gas Drainage & Ground Control of Deep Mines, Henan Polytechnic University, Jiaozuo 454000, China*
[3]*School of Architecture & Civil Engineering, Liaocheng University, Liaocheng 252059, China*
[4]*Beijing Tiandi Huatai Mining Management Co., Ltd.,Beijing 100013, China*

(*Received July 18, 2023, Revised January 7, 2024, Accepted February 7, 2024*)

Abstract. This study concentrates on the 301 comprehensive caving working face, notable for its considerable mining height. The roof model is established by integrating prior geological data and the latest borehole rock stratum's physical and mechanical parameters. This comprehensive approach enables the determination of lithology, thickness, and mechanical properties of the roof within 50 m of the primary mining coal seam. Utilizing the transfer rock beam theory and incorporating mining pressure monitoring data, the study delves into the geometric parameters of the direct roof, basic roof movement, and roof pressure during the initial mining process of the 301 comprehensive caving working face. The direct roof of the mining working face is stratified into upper and lower sections. The lower direct roof consists of 6.0 m thick coarse sandstone, while the upper direct roof comprises 9.2 m coarse sandstone, 2.6 m sandy mudstone, and 2.8 m medium sandstone. The basic roof stratum, totaling 22.1 m in thickness, includes layers such as silty sand, medium sandstone, sandy mudstone, and coal. The first pressure step of the basic roof is 61.6 m, with theoretical research indicating a maximum roof pressure of 1.62 MPa during periodic pressure. Extensive simulations and analyses of roof subsidence and advanced abutment pressure under varying working face lengths. Optimal roof control effect is observed when the mining face length falls within the range of 140 m-155 m. This study holds significance as it optimizes the working face length in thick coal seams, enhancing safety and efficiency in coal mining operations.

Keywords: optimization of the working face length; roof parameters; stope roof model; thick coal seam

1. Introduction

The coal mines in western China are renowned for their vast reserves of thick coal seams. These coal seams pose unique challenges in terms of extraction, and as a result, coal mining enterprises have adopted the method of top coal caving mining to effectively exploit these resources (Brady and Brown 2006, Le *et al.* 2019, Wang *et al.* 2020, Chen *et al.* 2023). The successful application of top coal caving mining in Russia in the 1940s drew attention to its potential benefits, leading to its subsequent adoption in China during the 1980s. Since then, the method has become widespread in the country, particularly in the coal-rich regions of western China. Its effectiveness in extracting coal from thick seams, coupled with its productivity, cost-efficiency, and safety considerations, has cemented its status as a preferred mining technique in the region (Xie *et al.* 1999, Cheng *et al.* 2019a, b).

The primary cause of roof collapse in faces with large mining heights is the stress exerted by the surrounding rock (Genis *et al.* 2018, Jaouhar *et al.* 2018, Rajwa *et al.* 2019).

The alteration in ground pressure, resulting from stress, has a significant influence on the condition of the working face's roof. By comprehending the pattern of ground pressure variation on the working face and integrating it with the movement parameters of the face, it is possible to determine optimal parameters for each working face and optimize the mining parameters for high mining height faces (Islam and Shinjo 2009, Guo *et al.* 2017). Hence, research on ground pressure induced by stress has become a fundamental and pivotal focus in coal mine safety research, bearing immense significance for ensuring the safety of working faces (Oh *et al.* 2019, Ibishi *et al.* 2022, Wang *et al.* 2022, Wang *et al.* 2023).

Top coal caving with large mining height is a highly effective method for mining thick coal seams, although it poses safety hazards due to the inherent instability of mine pressure. To address this issue, scholars have dedicated significant efforts (Bai *et al.* 2017, Babanouri and Sarfarazi, 2018, Ji *et al.* 2021, Ji *et al.* 2022). For instance, Yasitli and Unver (2005) conducted a study on the Omerler Underground Mine in Turkey, where they employed 3D simulation using FLAC3D to examine the top coal caving mechanism. Their findings emphasized that the cavability

*Corresponding author, Ph.D.
E-mail: 15610451523@163.com

ISSN: 2005-307X (Print), 2092-6219 (Online)

of the top coal layer is a critical factor determining the success of top coal mining. Understanding the cavability of the top coal layer is particularly crucial. The cavability of the top coal layer determines its susceptibility to caving and plays a key role in the overall success and safety of the mining process(Liu *et al.* 2019a, b, Li *et al.* 2020).

During the investigation of roof caving, Le *et al.* (2017) proposed the utilization of indicators that comprehensively capture the caving characteristics. In the analysis of strata caving behavior, Khanal, Adhikary *et al.* (2011) discovered that most rocks exhibit similar failure modes and compression collapse conditions. To gain a more comprehensive understanding of working face conditions, Vakili and Hebblewhite (2010) established a novel evaluation standard for caving properties. In the realm of mine pressure prediction, Alehossein and Poulsen (2010) developed a new yield function, which was employed to forecast mine pressure. The predictions derived from this function were subsequently validated through Particle Flow Code (PFC) modeling. Recognizing the insufficiency of stress analysis in existing underground mining face models, Coggan *et al.* (2012) emphasized the need for a thorough stress analysis in these models. To address this gap, Majdi, Hassani, and Nasiri (2012) formulated five novel mathematical models to determine the height of the stress zone under longwall coal mining. The reliability and validity of these models were successfully verified.

Dychkovskyi *et al.* (2022) posit that the formation of the support pressure zone is contingent upon the lithology, geological structure, and physical characteristics of the carbon-bearing strata. Vu (2022) identifies two main research directions for reducing roof collapse in working faces: mitigating the influence of mine pressure and enhancing the mechanical properties of rock strata. Meanwhile, Malashkevych *et al.* (2022) propose a novel mining technology involving gangue accumulation in goaf, offering insights into safe mining practices for working faces. Furthermore, Smoliński *et al.* (2022) predict that the presence of undercut rocks within the mined-out space can lead to pressure drop and extraction drifts in longwall faces. Expanding the research scope, Castelli *et al.* (2021) conduct a study on the dynamic response of a fully coupled soil-structure system utilizing the PLAXIS three-dimensional numerical program.

In summary, the current research on fully mechanized caving mining in large mining height working faces lacks comprehensive investigation due to the similarity of failure modes among most rocks. While the previous study provides valuable insights and guidance specific to the aforementioned mining context, its limitations should be acknowledged. Future research should explore the extension of findings to other mining scenarios and consider factors beyond those addressed in this particular investigation. By doing so, a more comprehensive understanding of fully mechanized caving mining in various settings can be achieved. To address this research gap, this study utilizes field data from the 301 working face of Changchunxing Mine. The research employs theoretical calculations to determine the rock structure and rock pressure of the working face. Furthermore, numerical simulations are conducted to analyze the relationship between roof subsidence under pressure and the length of the working face, with the aim of optimizing the working face length. The research methodology employed in this study provides a theoretical foundation for optimizing the working face of fully mechanized caving faces with large mining heights. This aspect of the research holds significant importance. However, it is important to note that this study's applicability is limited to fully mechanized caving faces with large mining heights and may not be universally applicable to other mining scenarios. But the approach of establishing a roof failure model by integrating measured mining pressure data, can be applied as a reference in mining areas with similar production conditions.

2. Background

2.1 Geological background

The Changchunxing Coal Mine is owned by Shanxi Coal Import and Export Group. The mining field covers an approximate area of 20 km^2. The integrated annual production capacity of the mine is around 2.4 million tons per year, with a design service life of 67 years. The mining field is specifically located in Zuoyun County, Datong City, Shanxi Province, China. It benefits from convenient transportation infrastructure in the area. The Changchunxing Coal Mine belongs to the Datong Coalfield, which is characterized by a low mountainous and hilly terrain. The surface is predominantly covered by loess, with sparse vegetation and the development of numerous gullies and valleys.

Fig. 1 illustrates the location, layout, and regional histogram of the 301 working face. The 301 working face in Changchunxing Coal Mine has a length of 230 m. The coal seam being mined has a thickness of 10.25 m and a dip angle of 2°. In addition to the main roadway, there are two conveying and return air roadways in the working face, positioned at a 45° angle with respect to the main roadway within the panel.

According to the preliminary geological exploration data, it is known that the rock strata in the research area are stably present. This paper summarizes the borehole column chart of the B12 borehole within the 301 working face, further referencing the physical and mechanical parameters of the rock strata at the same horizon as the B12 borehole from the geological data obtained in the early stages of mine development. This process helps determine the lithology, thickness, and mechanical properties of the rock layers within the 50m range of the 22 coal roof in the B12 borehole. Therefore, it can be affirmed that the parameters in Table 1 can essentially reflect the rock strata characteristics of the working face. The specific details are provided in Table 1.

2.2 Mining pressure monitoring system

As shown in Fig. 2 the mine pressure monitoring system can be divided into two parts: the above part and the underground part.

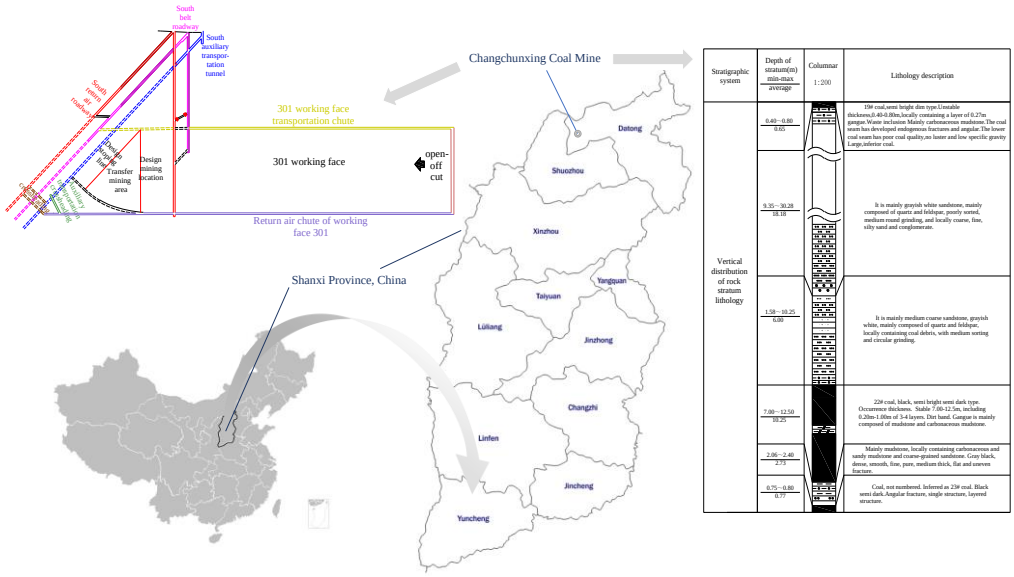

Fig. 1 Layout and regional histogram of 301 working face

Table 1 Rock physical and mechanical properties test results of 22# coal seam in B12 borehole

Serial number	Lithology	Layer thickness /m	Cumulative thickness above coal seam/m	Buried depth /m	Tensile strength/MPa	Compressive strength/MPa
16	Medium sandstone	9.90	58	194.6	0.97	23.9
15	Fine sandstone	2.80	48.1	197.4	1.13	44.1
14	Sandy mudstone	2.60	45.3	200	0.81	42.3
13	Fine sandstone	6.08	42.7	206.1	1.13	44.1
12	18 coal	1.2	36.62	207.3	——	——
11	Sandy mudstone	4.82	35.42	212.1	0.81	42.3
10	Medium sandstone	3.6	30.6	215.7	0.97	23.9
9	Sandy mudstone	2.33	27	218.0	0.81	42.3
8	19 coal	0.49	24.67	218.5	——	——
7	Sandy mudstone	1.18	24.18	219.7	0.81	42.3
6	Medium sandstone	0.8	23	220.5	0.97	23.9
5	Siltstone	1.6	22.2	222.1	1.84	58.4
4	Medium sandstone	2.8	20.6	224.9	0.97	23.9
3	Sandy mudstone	2.6	17.8	227.5	0.81	42.3
2	Coarse sandstone	9.2	15.2	236.7	0.97	23.9
1	Coarse sandstone	6.0	6.0	242.7	0.65	17.3
——	22 coal	9.5	——	252.2	——	——

The underground part is mainly divided into four substations: roof pressure monitoring, roof separation monitoring, bolt stress monitoring and borehole stress monitoring. The above part is mainly divided into two parts: data processor and mine office network. When the system is running, the four monitoring substations in the underground are connected to the information transmission interface above the mine through their respective communication substations, so as to summarize the real-time monitoring data to the data processor, and then the data processor analyzes the data and transmits it to each office network of the mine. Finally, the mining pressure is expressed in real time through the office network monitor above the mine, so as to achieve the purpose of real-time monitoring of mining pressure.

The working face pressure monitoring adopts the KJ564 mine compaction online monitoring system produced by Qingdao Benmo Rock Control Technology Co., Ltd. The actual distribution of the system area is shown in Fig. 3.

After statistical analysis of the monitoring data of each area of the working face, the corresponding roof movement law and ground pressure behavior law can be obtained.

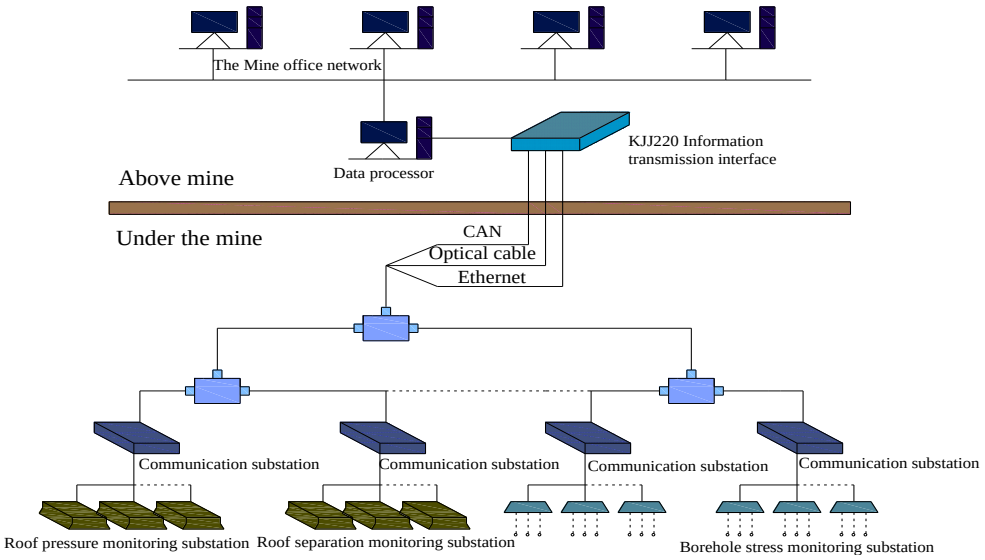

Fig. 2 Working resistance monitoring system

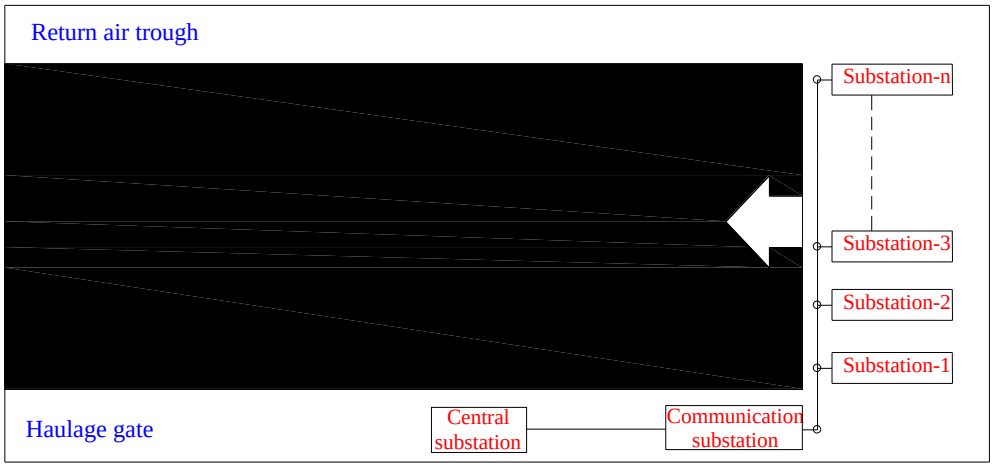

Fig. 3 Layout of measuring area in monitoring system

3. Analysis

3.1 Motion parameters of direct roof

3.1.1 Rock formation analysis

Due to the use of top coal caving mining technology, the top coal will collapse in the goaf. According to the work records of on-site workers in 301 working face, the working face starts to release coal at about 30 m away from the cut-hole. At this time, the failure height of the roof will inevitably increase with the increase of the lower space. The thickness of the caving rock layer is calculated according to the following formula (Song 1988, Tan 2021)

$$M_Z = \frac{h + \eta T - S_A}{K_A - 1} \tag{1}$$

In the formula:M_z—Direct top thickness, m;

h —Mining height, 3.5 m;

η —Recovery rate of top coal, 75%;

T —Thickness of Top coal, taken as 6.75 m;

S_A—Settlement value of main roof in contact with gangue, taken as S_A =(0.25~0.3)H, H=h+ηT;

K_A —Coefficient of rock fragmentation and expansion, taken as 1.3.

Calculated by substituting parameters M_z = 18.7 ~ 20 m. According to the rock stratum structure diagram of the working face, there may be five layers of rock stratum constituting the direct roof, namely roof ① ~ ⑤.

According to the roof collapse period (initial collapse / periodic collapse) and different roof treatment methods, the collapse step distance of direct roof can be calculated by two different methods:

Method 1: In the case of no forced coal caving at the cut-hole, the first caving step of the direct roof shall be calculated by using the embedded beams at both ends, which shall be calculated according to formula (2) (Song 1988, Tan 2021)

$$L_{0Z} = \sqrt{\frac{2M_Z[\sigma_t]}{\gamma_Z}} \tag{2}$$

Table 2 Calculated value of immediate roof hanging coefficient in 301 working face

Serial number	Lithology	Layer thickness /m	Tensile strength /MPa	Compressive strength /MPa	Initial caving step/m	Periodic caving step /m	Overhang distance /m	Hanging roof coefficient
⑤	Siltstone	1.6	1.40	39.5	13.40	5.5	0	1
④	Medium sandstone	2.8	0.97	23.9	14.74	6.0	0	1
③	Sandy mudstone	2.6	0.81	42.3	12.98	5.3	0	1
②	Coarse sandstone	9.2	0.97	23.9	26.7	10.9	4.64	3.0
①	Coarse sandstone	6.0	0.65	17.3	17.66	7.2	0.94	1.3
——	22 coal	9.5	——	——	21.1	8.6	2.34	1.9

In the formula: M_z —Thickness of direct top single rock layer, m;

σ_t —Tensile strength of direct roof single rock layer, MPa;

γ_Z —The unit weight of single rock layer on the direct roof is 25 kN/m^3;

L_{0Z} —The first caving step of the direct roof, m.

Method 2: Calculate the periodic caving step of the direct roof with cantilever beam according to formula (3) (Song 1988, Tan 2021)

$$L_Z = \sqrt{\frac{M_Z[\sigma_t]}{3\gamma_Z}} \tag{3}$$

In the formula: L_Z —The periodic caving step of the direct roof, m.

Since the cut-hole of 301 working face is not subject to forced caving, the initial collapse step of each layer that may form the direct roof is still calculated according to the embedded beams at both ends, and the periodic caving step is calculated according to the cantilever beam.

Hanging roof coefficient: the hanging roof coefficient of each layered rock stratum of direct roof is calculated according to the following formula (4) and (5) (Song 1988, Tan 2021)

$$f_Z = \frac{1}{2n_z}\left(\frac{L_K + L_S}{L_K}\right)^2 \tag{4}$$

$$n_Z = \frac{S_0}{L_K} \tag{5}$$

In the formula: S_0—Distance between action point of support resultant force and coal wall; For fully mechanized caving support, generally S_0 =0.5L_K, then n_Z = 0.5;

L_K—The roof control distance of support, which have minimum $L_{K\min}$ =5.86 m and maximum $L_{K\max}$ =6.66 m, here take the average L_K =6.26 m;

f_z—Hanging roof coefficient.

The calculation results of collapse step distance, suspended roof distance and suspended roof coefficient of each layer that may form the direct roof are listed in Table 2.

Table 3 The statistical table of Initial pressure value and pressure position of 301 working face

Support number		Support pressure value /kN		Incoming pressure position
		Before pressure	When pressing	
Initial roof pressure	20#	4374	10212	31.2
	30#	4356	13085	31.6
	50#	3299	11215	32.5
	55#	3612	10562	29.6
	60#	3802	13002	30.1
	65#	3293	11976	31.6
	70#	3410	13521	31.3
	90#	3435	10421	30.2
	110#	4410	11400	31.6
Average value		3776	11710	31.1

3.1.2 Thickness calculation and lithology analysis

Because the motion characteristics of the direct roof are different in the initial collapse, it can be divided into upper direct roof and lower direct roof to calculate separately.

(1) The thickness of lower direct roof

See Table 3 for the summary of pressure at and before the initial pressure appearance in the initial mining stage of 301 working face.

Before the initial pressure appearance of the roof, the average value of the roof pressure is 3776 kN (converted into the support strength of 0.34 MPa). Considering that the support bears the force of the top coal and part of the caving direct top rock stratum at this time, then

$$P_0' = \gamma_T T + \gamma_Z M_Z \tag{6}$$

In the formula: P_0' —Support load before initial movement of roof, 0.34 MPa;

M_z—Thickness of direct roof strata of partial caving, m.

Calculated by substituting parameters: M_z =9.82 m.

If the direct roof thickness of caving is: □ + □ = 15.2 m, substitute formula (6) to calculate P_0' = 0.47 MPa ＞ 0.34 MPa.

According to the rock structure of the working face (see Table 2), the direct roof thickness of some caving can only be the coarse sandstone layer with a thickness of 6.0 m above the top coal. Substituting M_z = 6.0 m into formula (6),

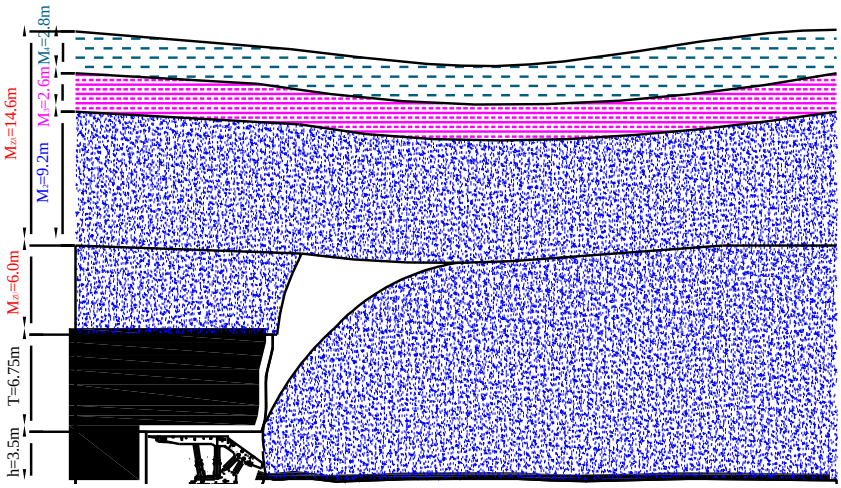

Fig. 4 Roof structural mode of immediate roof

it is calculated that $p_0' = 0.25$ MPa is slightly less than 0.34 MPa, which is caused by the pressure increment caused by the slow subsidence of the roof rock above the lower direct roof.

To sum up, the lower direct roof is a coarse sandstone layer with a thickness of 6.0 m, that is the lower direct roof M_{ZU}= 6.0 m.

(2) The thickness of upper direct roof

It can be seen from Table 4 that when the working face is mined to about 31.1 m (excluding the cut-hole width of 9.0 m), the roof collapses for the first time. At this time, the average roof pressure is 1.11 MPa. At this time, the measured parameters can be used to back calculate the initial collapse thickness of the upper direct roof rock, namely

$$P_T = \gamma_T T + \gamma_Z M_{ZU} + \frac{\gamma_Z M_{ZA} L_{0ZA}}{2L_K} \tag{7}$$

In the formula: P_r—Support load during initial collapse of upper direct roof, P_r =1.11 MPa;

γ_Z —Unit weight of roof rock stratum, taken as γ_Z = 25 kN/m^3;

M_{ZA} —Thickness of upper direct roof, m;

L_{0ZA} —Measured initial collapse step distance of upper direct roof rock, L_{0ZA} =31.1 m

Calculated by substituting parameters M_{ZA} = 13.9 m. That is, the thickness of the upper direct roof is 13.9 m. According to the rock structure of the working face (see Table 2), the upper direct roof consists of roof: □ + □ + □ = 14.6 m.

When the upper direct roof forms a combined movement from the roof □ + □ + □, substitute M_{ZA}= 14.6 m into formula (2) to calculate that the initial collapse step is L_{0ZA} = 33.7 m. The theoretical calculation is basically consistent with the measured parameters, which shows that the analysis of the thickness and structural characteristics of the direct roof is correct.

To sum up, the total thickness of the direct roof is M_z = 20.6 m, the lower direct roof is M_{ZU} = 6.0 m, and the upper direct roof is M_{ZA} = 14.6 m. The structural diagram of direct roof is shown in Fig. 4.

3.1.3 Periodic collapse

When the upper direct roof periodically collapses, substitute M_{ZA} = 14.6 m into formula (3), the calculated periodic collapse step distance is L_{ZA} = 13.7 m, and the measured average periodic collapse step of upper direct roof is 10.2 m. The theoretical calculation is basically consistent with the measured parameters.

From the above analysis, it can be seen that although the top points are in the upper and lower positions directly, the motion characteristics are different at the beginning of its collapse; In the process of periodic collapse, the measured periodic collapse steps of lower direct roof and upper direct roof of 301 working face are 7.2 m and 10.2 m respectively. Therefore, when the direct roof collapses periodically, the upper and lower direct roofs can be combined and analyzed as a whole.

The first collapse of the upper direct roof falls behind, and the direct roof enters the periodic collapse process. At this time, the load borne by the support is the top coal and all direct jacking forces. At this time, the minimum load borne by the support is

$$P_{min} = \gamma_T T + \gamma_Z M_Z \tag{8}$$

In the formula: M_Z —The total thickness of the direct roof, 20.6 m.

Calculated by substituting parameters: $P_{\min}$ =0.61 MPa.

The maximum load borne by the support is

$$P_{max} = \gamma_T T + \sum_{i=1}^{4} \gamma_{Zi} M_{Zi} f_{Zi} \tag{9}$$

In the formula: f_{Zi} —Hanging roof coefficient of each stratum of direct roof (see Table 3). Calculated by substituting parameters P_{max} =1.11 MPa.

See Table 4 for various parameters of direct roof during initial mining of 301 working face.

The bearing diagram of support during periodic collapse of direct roof is shown in Fig. 5.

Table 5 Measured and theoretical values of the composite structure for the basic roof strata

P_T/MPa	Combined rock stratum	M_E/m	Measured value C_0/m	Theoretical calculation value $C_0^{'}$/m	Measured and Theoretical Difference /m
1.12	roof 5~12	16.02	63.8	48.6	15.2
	roof 5~13	22.1	46.2	57.0	10.8
	roof 5~14	24.7	41.4	60.3	18.9
	roof 5~15	27.5	37.1	63.6	26.5
1.29	roof 5~12	16.02	85.0	48.6	36.4
	roof 5~13	22.1	61.6	57.0	4.6
	roof 5~14	24.7	55.1	60.3	5.2
	roof 5~15	27.5	49.5	63.6	14.1

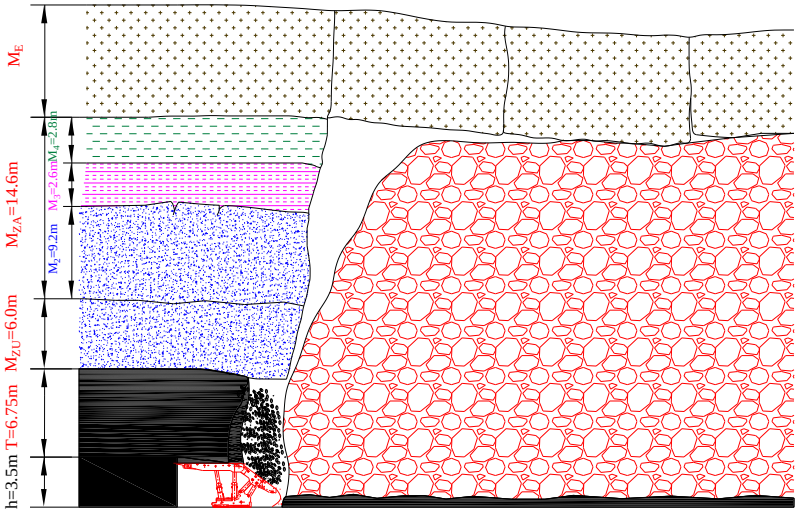

(a) The support bears the minimum load

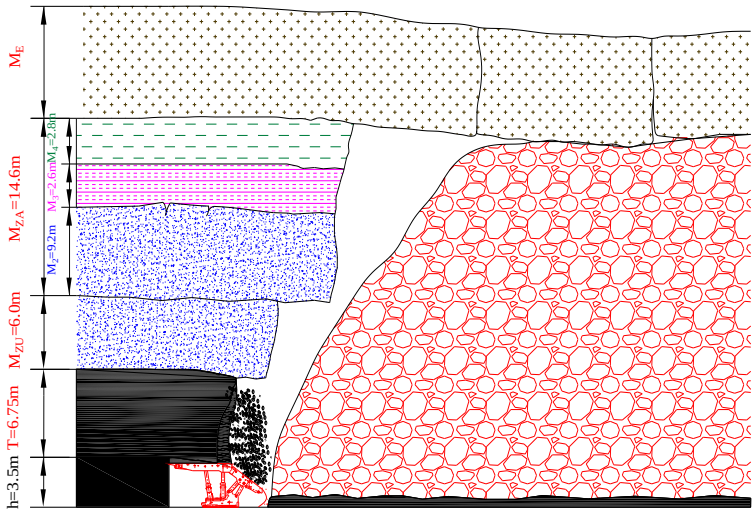

(b) The support bears the maximum load

Fig. 5 Model diagram of support bearing structure during periodic collapse of direct roof

To sum up, before the first pressure of the basic roof, the support mainly bears the static load of the top coal and the direct roof strata, and the pressure when the upper direct roof is suspended and collapsed periodically is the main source of the support load before the initial pressure of the basic roof.

3.2 Motion parameters of basic roof

3.2.1 First pressure of basic roof

During the 100m advancement of the working face, it is monitored that the roof pressure increases for many times. During the continuous pressure appearance, the roof

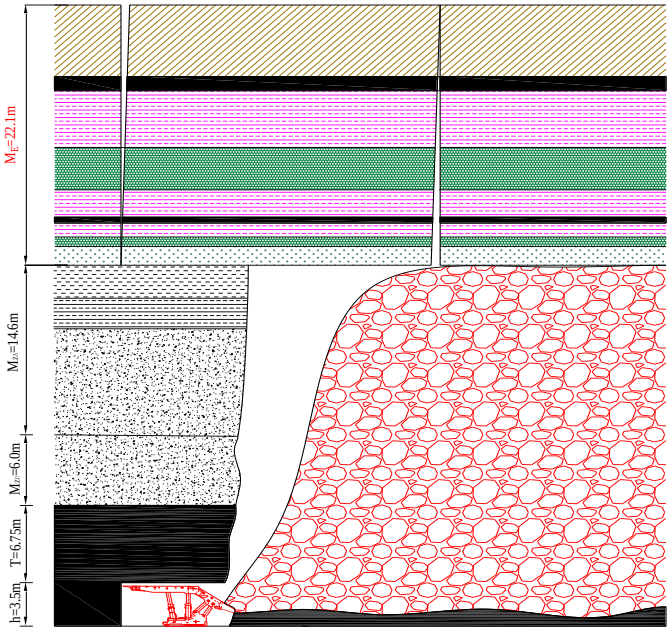

Fig. 6 Roof structural mode in initial mining period

pressure is 1.10 ~ 1.29 MPa, with an average of 1.12 MPa. According to the above analysis, the maximum roof pressure during the periodic collapse of the direct roof is 1.11 MPa. Therefore, if most of the roof pressure is greater than 1.11 MPa during a continuous pressure appearance, it is likely that the primary pressure of the basic roof has occurred.

The thickness of the basic roof strata is inversely calculated according to the measured support load

$$P_T = A + \frac{\gamma_E M_E C_0}{2K_T L_K} \tag{10}$$

In the formula: P_r—Measured support load, MPa;

A—When the top coal and direct roof strata have no suspended roof, taken as 0.61 MPa;

γ_E—Volume weight of basic roof strata, taken as 25 kN/m^3;

M_E—Thickness of basic roof, m;

C_0—First pressure step distance of basic roof, m;

K_r—Rock proportion distribution coefficient, taken as 4.0.

By substituting the parameters into the formula (10), the measured values of the first weighting step C_0 of the basic roof under different measured support loads can be obtained.

The theoretical calculated values of the first weighting step of the basic roof can be calculated by formula (11)

$$C_0^{'} = \sqrt{\frac{2M_E[\sigma_r]}{\gamma_E}} \tag{11}$$

In the formula: σ_r—Tensile strength of basic roof, taken as 0.8 MPa.

The measured values and theoretical calculated values of the combined structure of basic roof strata under different values of P_r are listed in Table 5.

According to the statistical results of Table 5:

(1) When P_T = 1.12 MPa and the basic roof combined structure is M_E = 22.1 m, the measured value is 46.2 m, the theoretical value is 57.0 m. The measured and theoretical difference of the first pressure step distance of the basic roof is the smallest, which is 10.8 m.

(2) When P_r = 1.29 MPa and the basic roof combined structure is M_E = 22.1 m, the measured value is 61.6 m, the theoretical value is 57.0 m. The measured and theoretical difference of the first pressure step distance of the basic roof is the smallest, which is 4.6 m.

From the above analysis, it can be seen that when the measured working face advances 46.2 m, the roof pressure is stable and in the process of non-continuous pressure appearance; When the measured working face is mined to 61.6 m, the roof pressure is in the process of continuous pressure appearance.

To sum up, the thickness of the basic roof rock stratum is M_E = 22.1 m, which is composed of 1.6 m thick silty sandstone, 0.8 m thick medium sandstone, 1.18 m thick sandy mudstone, 0.49 m thick 19 coal, 2.33 m thick sandy mudstone, 3.6 m thick medium sandstone, 4.82 m thick sandy mudstone, 1.2 m thick 18 coal and 6.08 m thick fine sandstone. The first pressure step of the basic roof is 61.6 m.

Therefore, the roof structure model of the working face during the pressuring of the basic roof is shown in Fig. 6.

3.2.2 Periodic pressure of basic roof

By substituting M_E = 22.1 m into formula (3), it is calculated that the periodic pressure step distance of the basic roof is C = 23.3 m.

When the basic roof is pressed periodically, the load borne by the support is

$$P_T = A + \frac{\gamma_E M_E C}{K_T L_K} \tag{12}$$

Table 6 Motion parameters of basic roof in 301 working face

Total thickness /m	Layer thickness /m	lithology	Initial pressure step /m	Periodic pressure step /m
	1.6	Siltstone		
	0.8	Medium sandstone		
	1.18	sandy mudstone		
	0.49	19 coal		
22.1	2.33	sandy mudstone	61.6	23.3
	3.6	Medium sandstone		
	4.82	sandy mudstone		
	1.2	18 coal		
	6.08	fine sandstone		

Table 7 Mechanical parameters of different rock stratum

Serial number	Lithology	Layer thickness/m	Bulk /10^9Pa	Tangential stress /10^9Pa	Friction /	Tension /10^6Pa	Density /10^3kg/m^3	Cohesion /10^6Pa
⑨	Siltstone	21	12	9	39	2.7	3.7	13.2
⑧	Sandy mudstone	3	7	4	34	1.7	2.6	6.7
□	Medium sandstone	15	19	8	37	1.6	3.8	11.9
□	Granular sandstone	3	13	10	33	2.2	2.6	8.9
□	Medium coarse sandstone	7	15	11	36	2.6	2.9	10.3
□	22 coal	9.25	3	1.6	28	0.8	1.3	1.2
□	Mudstone 1	3	4.5	3.2	26	1.9	2.39	2.2
□	Fine sandstone	6	10	7	31	2.2	2.5	6.1
□	Mudstone 2	8	4.2	3.1	35	3.7	2.1	5.8

In the formula: C—The theoretical calculation value of step distance of basic roof periodic pressuring, namely 23.3 m.

Calculated by substituting parameters: P_T =1.12 MPa.

According to the above analysis, the first caving step distance of direct roof is 31.1 m, and the periodic caving step distance of direct roof is 10.2 m; The first pressure step distance of the basic roof is 61.6 m, and the periodic pressure step distance of the basic roof is 23.3 m. Therefore, during the mining period of the working face, when the direct roof periodic collapses in the form of suspended roof, the periodic pressure of the basic roof may happen. At this time, the mine pressure behavior of the working face is greater than that caused by the simple direct roof suspended roof collapse and the periodic pressure of the basic roof. At this time, the maximum pressure during basic roof periodic pressure

$$P_{Tmax} = \gamma_T T + \sum_{i=1}^{4} \gamma_{Zi} M_{Zi} f_{Zi} + \frac{\gamma_E M_E C}{K_T L_K} \tag{13}$$

Calculated by substituting parameters P_{Tmax} =1.62 MPa.

From the above analysis, it can be seen that when the direct roof periodic collapse coincides with the basic roof periodic pressure, the maximum roof pressure that may be generated is 1.62 MPa, exceeding the rated maximum support strength of the hydraulic support of the working face is 1.23 MPa, and whether this limit situation will occur in the actual propulsion process of the working face depends on the roof movement.

According to the above calculation, analysis and summary, the motion parameters of basic roof are shown in Table 6.

4. Mining pressure simulation of different working face lengths

4.1 Model building

The FLAC3D numerical simulation model is established based on the geological data and mining conditions of 301 working face of Changchunxing coal mine. The rock mechanical parameters of each stratum are shown in Table 7. The boundary conditions of the model include: constraints on horizontal displacement in the left and right directions, fixed constraints in the lower part, loading equivalent forces in the upper part, the stage analysis method of gradual excavation is used to simulate. The length, width and height of the model correspond to the X, Y and Z directions, and the specific sizes are 360 m, 390 m and 63 m. The overall model consists of 15851 grids and 93600 nodes. The vertical height direction is mainly composed of three layers: floor (10 m) and coal seam

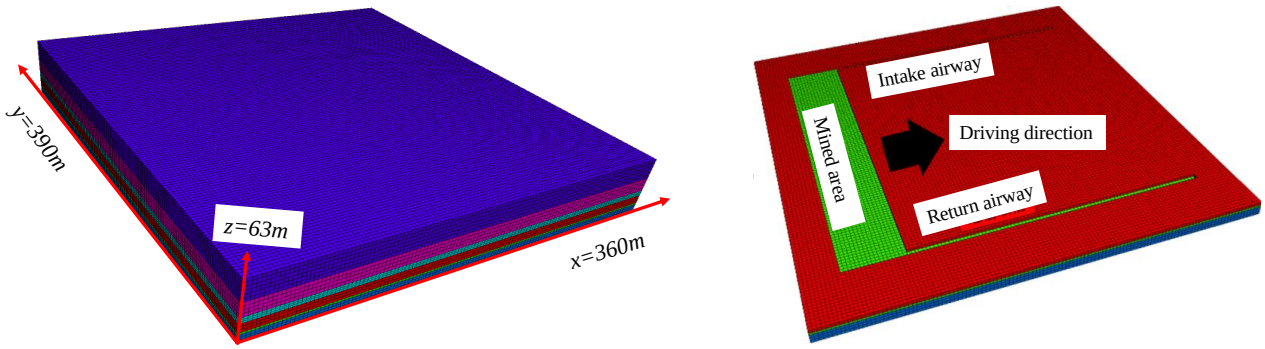

(a) Side view of the model (b) Excavdiagram of working face

Fig. 7 Schematic diagram of simulation model

(thickness 10.25 m), roof (total thickness of direct roof is 20.6 m, and total thickness of basic roof is 22.1 m). The diagrammatic drawing of the model is shown in Fig. 7.

In order to eliminate the boundary effect, a 25 nm reserve coal pillar is reserved along the X and Y directions during model excavation. In order to facilitate the observation of the movement of the overlying strata of the working face, the height of each square grid is about 1 m along the vertical direction, the load applied on the upper boundary is calculated according to the mining depth of 220 m, and the support strength of 1.11 MPa is applied to the upper part of the working face roof as the maximum support capacity of the support.

The simulation comprises two stages. In the initial stage, macroscopic mine pressure manifestation during the advancement of working faces with different lengths and various advancing processes was simulated. Building upon these findings, 100 m was established as a critical advancement threshold, leading to a comparative analysis of roof convergence for working faces of varying lengths below this threshold. Based on the measured face length base (approximately 200 m), it is determined that the working face length in the simulation starts from 140 m and takes 30 m as the gradient, taking 140 m, 170 m, 200 m, 230 m and 260 m in turn. The working face is excavated for 200 m along the strike direction of the coal seam, and the advancing distance is expressed in T. The excavation is carried out in four steps to study the variation of the macroscopic mining pressure behavior of the working face during the excavation process. The top coal release rate is calculated as 75%. In the second stage, a simulation study was conducted on the advance abutment pressure of working faces of different lengths during the advancement of 100 m. The foundational model for this stage mirrors the one established in the initial simulation phase.

4.2 Simulation results and analysis

The roof vertical displacement in the simulation results is studied to analyze the macroscopic mining pressure behavior law under different working face lengths, and then the roof subsidence is used to verify the roof control effect of the existing support on the roof, so as to optimize the working face length according to the roof control effect.

4.2.1 Analysis of roof subsidence

The maximum roof subsidence in the middle of the working face under different advancing distances corresponding to different working face lengths was shown in Fig. 8.

It can be seen from Fig. 8 that the vertical displacement of the roof will increase with the increase of the length of the working face and the increase of the advancing distance.

The maximum roof subsidence in the middle corresponding to different working face lengths and different advancing distances is listed in Table 8, and the roof subsidence curve chart is drawn according to the results, as shown in Fig. 9.

According to the cloud images, statistical table and curve chart analysis of roof subsidence with different advancing distances under different mining face lengths:

(1) In the process of advancing 200 m, for the working face with fixed length, with the continuous advancement of the working face direction, the change rate of roof subsidence changes from large to small, and finally tends to be stable.

(2) Compared with the roof subsidence of working faces with different lengths under the same advancing distance, the roof subsidence tends to increase with the increase of working face length.

(3) It can be seen from the observation curve chart that the advancing distance is from 50 to 100 m, the change rate of roof subsidence is large, the change rate of roof subsidence is stable after the advancing distance of the working face is greater than 100 m.

Based on the above conclusions, we take 100 m as a critical value of the advancing distance to compare and analyze the roof subsidence of different working face lengths when the advancing distance is 100 m, 150 m and 200 m.

In the method of determining the support capacity of the simulated support, the support capacity can be reflected in the roof control effect, and the roof subsidence of the working face can be used as the main discrimination index of the support capacity. According to the actual situation of Changchunxing coal mine, the discrimination standard suitable for Changchunxing coal mine is established and the section threshold is selected. The specific standard is shown in Table 9.

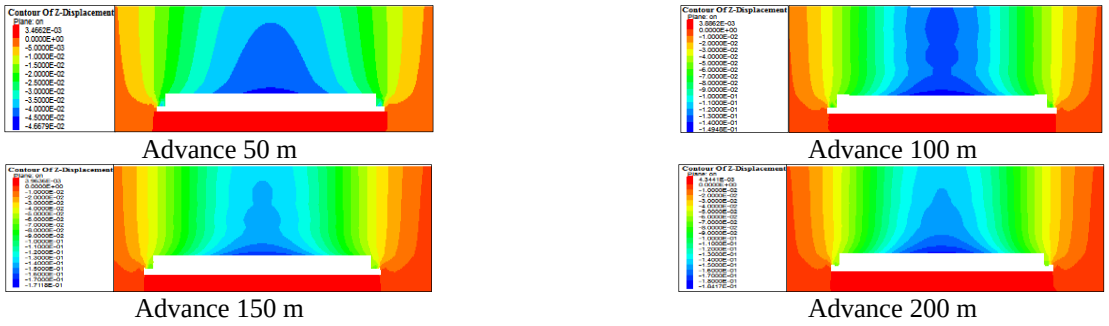

(a) Working face length 140 m

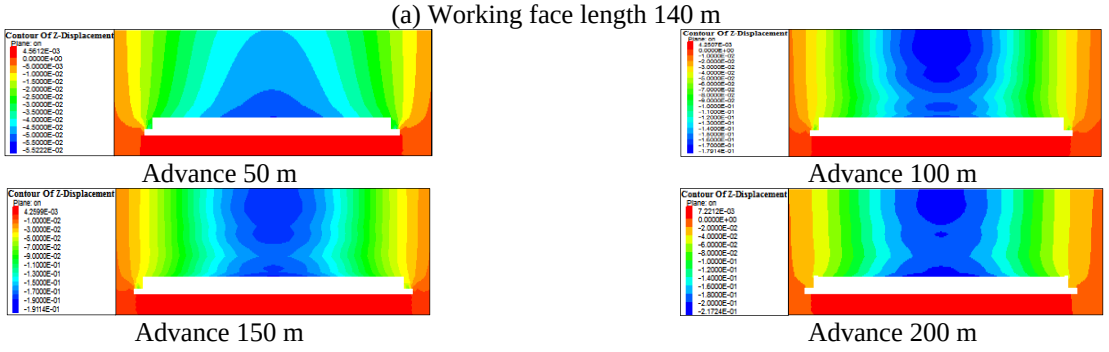

(b) Working face length 170 m

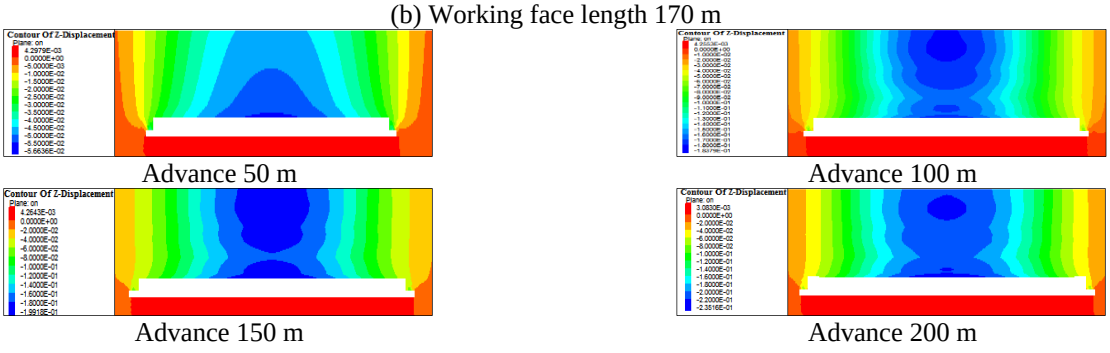

(c) Working face length 200 m

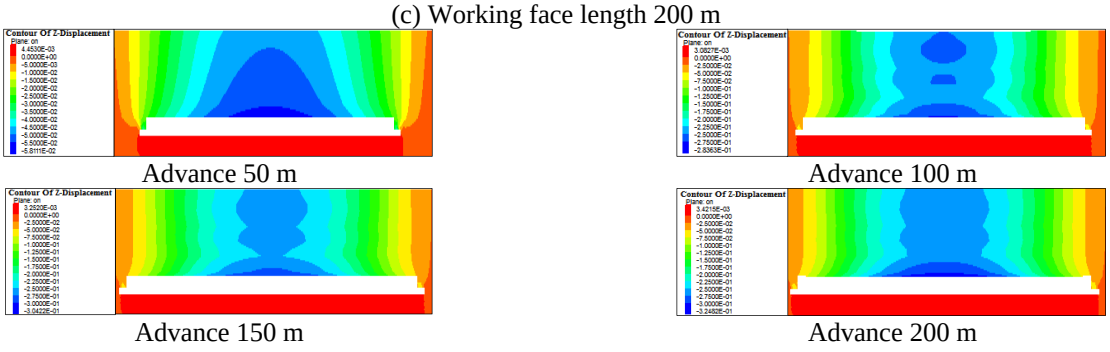

(d) Working face length 230 m

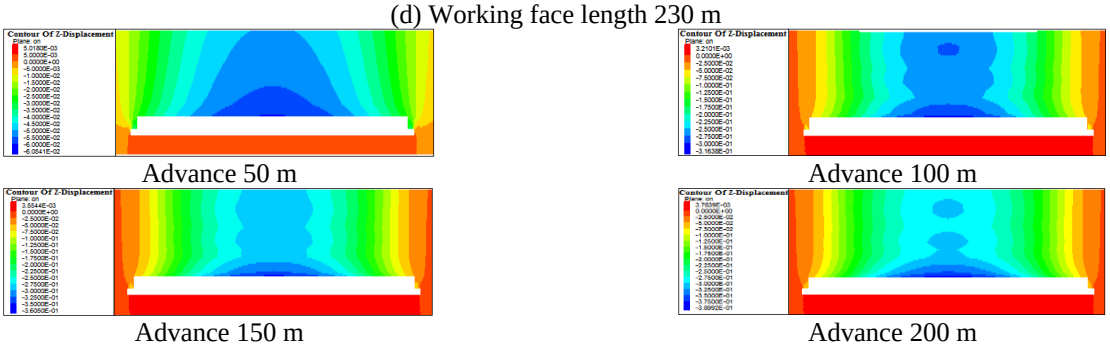

(e) Working face length 260 m

Fig. 8 Cloud images of roof subsidence under different face lengths and different advancing distances

Table 8 Statistical table of the maximum roof subsidence of the working faces with different lengths

working face length/m	Maximum subsidence of roof/mm			
	T=50 m	T=100 m	T=150 m	T=200 m
140	45	149	171	184
170	55	179	191	217
200	56	183	199	235
230	58	283	304	324
260	60	316	360	390

Table 9 Roof control effect standard of working face

Roof control effect of mining face	Best	Good	Medium	Bad
Roof subsidence /mm	≤100	101~200	201~400	≥401

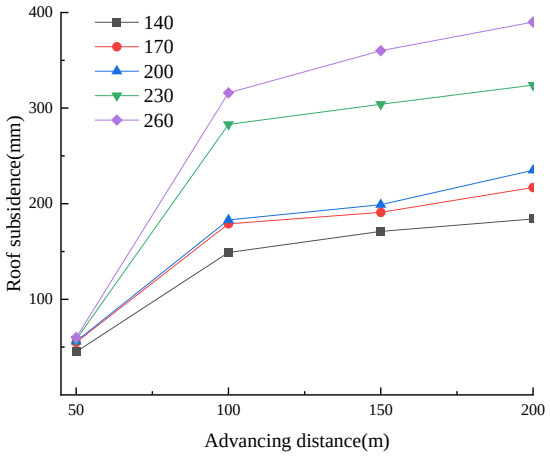

Fig. 9 Curve chart of roof subsidence

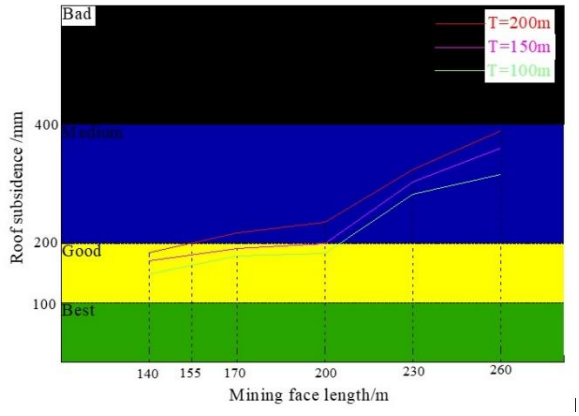

Fig. 10 Roof control effect standard corresponding to roof subsidence

According to Table 9, the roof control effect diagram corresponding to the roof subsidence under different working face lengths and different advancing distances can be drawn, as shown in Fig. 10. Only when the length of the working face is in the range of 140 m-155 m, the roof control effect under the three advancing distances of 100m, 150m and 200m all is "good". Therefore, the optimal length range of the working face studied in this paper should be 140 m-155 m.

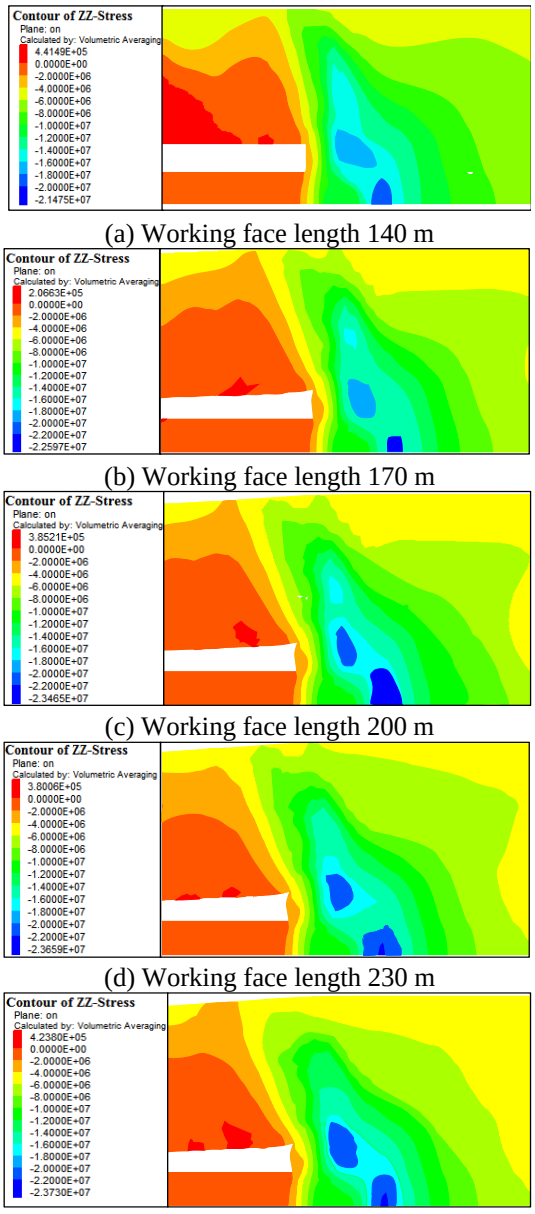

(a) Working face length 140 m

(b) Working face length 170 m

(c) Working face length 200 m

(d) Working face length 230 m

(e) Working face length 260 m

Fig. 11 The advanced abutment pressure in different working face length

4.2.2 Macroscopic mining pressure behavior law

The cloud diagram of the advance abutment pressure when advancing 100 m in different working face lengths is shown in Fig. 11. According to the Fig. 11, the specific value of the advance abutment pressure was listed in Table 10.

It can be seen from Fig. 11 and Table.10 that behind the working face is the goaf, which is in a state of unloading and does not exhibit stress concentration phenomena. Therefore, the stress distribution state behind the working face is generally not considered. Due to stress transfer, a stress concentration zone will appear in front of the working face, which is the focal area for potential damage. Analysis of the advancing support pressure contour maps for different lengths of working faces reveals that with the increase in face length, the peak value of the advancing

Table 10 Statistics of the advance abutment pressure in different working face length

Working face length/m	140	170	200	230	260
Advance abutment pressure/MPa	18.0	20.0	21.8	22.0	21.9

support pressure gradually increases, and the affected area of the advancing support pressure enlarges. When the face length exceeds 200 m, the advancing support pressure tends to stabilize, reaching a maximum of 22 MPa.

5. Conclusions

• The direct roof in the mining working face is categorized into the upper direct roof and lower direct roof. The lower direct roof is comprised of a robust 6.0 m thick layer of coarse sandstone. Contrastingly, the upper direct roof is a combination of 9.2 m coarse sandstone, 2.6 m sandy mudstone, and 2.8 m medium sandstone, presenting a cumulative thickness of 14.6 m.

• Prior to the initial pressurization of the basic roof, the support primarily sustains the static load exerted by the top coal and the direct roof strata. Notably, the support load during the periodic suspension and collapse of the upper direct roof constitutes a pivotal component of the overall support load before the basic roof's initial pressurization.

• The basic roof stratum exhibits a complex composition, featuring layers such as a 1.6 m silty sand layer, 0.8 m medium sandstone layer, 1.18 m sandy mudstone layer, 0.49 m 19 coal, 2.33 m sandy mudstone layer, 3.6 m medium sandstone layer, 4.82 m sandy mudstone layer, 1.2 m 18 coal, and 6.08 m fine sandstone layer, accumulating to a total thickness of 22.1 m. The theoretical exploration suggests a potential maximum roof pressure of 1.62 MPa during periodic pressure on the basic roof.

• Employing FLAC3D numerical simulation, the study delves into roof subsidence dynamics concerning varying mining face lengths under specific loads. As the advancing distance increases, roof subsidence stabilizes progressively. However, an observable escalating trend in roof subsidence becomes evident with an augmentation in the mining face length. Stability in the change rate of roof subsidence occurs when the mining face's advancing distance surpasses 100 m. Optimal roof control effectiveness is achieved within a mining face length range of 140 to 155 m.

Acknowledgments

This work was supported by the Natural Science Research Project of Anhui Educational Committee (2023AH051187), National Natural Science Foundation of China (52304198), Anhui Provincial Key Research and Development Project (2022m07020006), State and Local Joint Engineering Laboratory for Gas Drainage & Ground Control of Deep Mines (Henan Polytechnic University (No. SJF2208) and Anhui University Excellent Scientific Research and Innovation Team Project (2022AH010051).

References

Alehossein, H. and Poulsen, B.A. (2010), "Stress analysis of longwall top coal caving", *Int. J. Rock Mech. Min.*, **47**(1), 30-41. https://doi.org/10.1016/j.ijrmms.2009.07.004.

Bai, Q., Tu, S., Wang, F. and Zhang, C. (2017), "Field and numerical investigations of gateroad system failure induced by hard roofs in a longwall top coal caving face", *Int. J. Coal Geol.*, **173**, 176-199. https://doi.org/10.1016/j.coal.2017.02.015.

Babanouri, N. and Sarfarazi, V. (2018), "Numerical analysis of a complex slope instability: Pseudo-wedge failure", *Geomech. Eng.*, **15**(1), 669-676. https://doi.org/10.12989/gae.2018.15.1.669.

Brady, B. and Brown, E. (2006), *Rock Mechanics for underground mining*, Spring Ed., **1**. Netherlands. https://doi.org/10.1016/j.coal.2017.02.015.

Castelli, F., Grasso, S., Lentini, V. and Sammito, M.S.V. (2021), "Effects of soil-foundation-interaction on the seismic response of a cooling tower by 3D-FEM analysis", *Geosci.*, **11**(5), 200. https://doi.org/10.3390/geosciences11050200.

Chen, B. and Shen, B. and Jiang, H. (2023), "Shear behavior of intact granite under thermo-mechanical coupling and three-dimensional morphology of shear-formed fractures", *J. Rock Mech. Geotech. Eng.*, English edition, **15**(3), 15. https://doi.org/10.1016/j.jrmge.2022.04.006.

Cheng, Z. and Yang, S., Li, L. and Zhang, L. (2019). "Support working resistance determined on top - coal caving face based on coal -rock combined body", *Geomech. Eng.*, **19**(3), 255-268. https://doi.org/10.12989/gae.2019.19.3.255.

Cheng, Z. and Pan, W., Li, X. and Sun, W. (2019), "Numerical simulation on strata behaviours of TCCWF influenced by coal - rock combined body", *Geomech. Eng.*, **19**(3), 269-282. https://doi.org/10.12989/gae.2019.19.3.269.

Coggan, J., Gao, F.Q., Stead, D. and Elmo, D. (2012), "Numerical modelling of the effects of weak immediate roof lithology on coal mine roadway stability", *Int. J. Coal Geol.*, **90-91**, 100-109. https://doi.org/10.1016/j.coal.2011.11.003.

Dychkovskyi, R., Shavarskyi, I., Saik, P., Lozynskyi, V., Falshtynskyi, V. and Cabana, E. (2020), "Research into stress-strain state of the rock mass condition in the process of the operation of double-unit longwalls", *Dnipro Univ. Tech.*, **14**, 85-94. https://doi.org/10.33271/mining14.02.085.

Genis, M. and Akcin, H., Aydan, O. and Bacak, G. (2018), "Investigation of possible causes of sinkhole incident at the Zonguldak Coal Basin, Turkey", *Geomech. Eng.*, **16**(2), 177-185. https://doi.org/10.12989/gae.2018.16.2.177.

Guo, W.B., Tan, Y. and Bai, E.H. (2017), "Top coal caving mining technique in thick coal seam beneath the earth dam", *Int. J. Min. Sci. Tech.*, **27**(1), 165-170. https://doi.org/10.1016/j.ijmst.2016.11.005.

Ibishi, G., Genis, M. and Yavuz, M. (2022), "Post-pillars design for safe exploitation at Trepca hard rock mine (Kosovo) based on numerical modeling" *Geomech. Eng.*, **28**(5), 463-475. https://doi.org/10.12989/gae.2022.28.5.463.

Islam, M.R. and Shinjo, R. (2009), "Numerical simulation of stress distributions and displacements around an entry roadway with igneous intrusion and potential sources of seam gas emission of the Barapukuria coal mine, NW Bangladesh", *Int. J. Coal Geol.*, **78**(4), 249-262. https://doi.org/10.1016/j.coal.2009.03.001.

Jaouhar, E., Li, L. and Aubertin, M. (2018), "An analytical solution for estimating the stresses in vertical backfilled stopes based on a circular arc distribution", *Geomech. Eng.*, **15**(3),

889-898. https://doi.org/10.12989/gae.2018.15.3.889.

Ji, S.T.,He, H. and Karlovšek, J. (2021), "Application of superposition method to study the mechanical behaviour of overlying strata in longwall mining", *Int. J. Rock Mech. Min.*, 146. https://doi.org/10.1016/j.ijrmms.2021.104874.

Ji, S., Wang, Z. and Karlovšek, J. (2022), "Analytical study of subcritical crack growth under modeI loading to estimate the roof durability in underground excavation", *Int. J. Min. Sci. Tech.*, **32**(2), 11. https://doi.org/10.1016/j.ijmst.2021.08.006

Khanal, M., Adhikary, D. and Balusu, R. (2011), "Evaluation of mine scale longwall top coal caving parameters using continuum analysis", *Int. J. Min. Sci. Tech*., **21**(6), 787-796. (in Chinese) https://doi.org/10.1016/j.mstc.2011.06.027.

Le, T.D., Mitra, R., Oh, J. and Hebblewhite, B. (2017), "A review of cavability evaluation in longwall top coal caving", *Int. J. Min. Sci. .Tech*., **27**(6), 907-915. https://doi.org/10.1016/j.ijmst.2017.06.021.

Le, T.D., Zhang, C.G., Oh, J. and Mitra, R. (2019), "A new cavability assessment for Longwall Top Coal Caving from discontinuum numerical analysis", *Int. J. Rock Mech. Min.*, **115**, 11-20. https://doi.org/10.1016/j.ijrmms.2019.01.006.

Li, C. and Xie, J., He, Z., Deng, G. and Yang, B. (2020), "Case study of the mining-induced stress and fracture network evolution in longwall top coal caving", *Geomech. Eng*., **22**(2), 133-142. https://doi.org/10.12989/gae.2020.22.2.133.

Liu, F. and Silva, J., Yang, S., Lv, H. and Zhang, J. (2019), "Influence of explosives distribution on coal fragmentation in top - coal caving mining", *Geomech. Eng*., **18**(2), 111-119. https://doi.org/10.12989/gae.2019.18.2.111.

Majdi, A., Hassani, F.P. and Nasiri, M.Y. (2012), "Prediction of the height of destressed zone above the mined panel roof in longwall coal mining", *Int. J. Coal Geol*., **98**, 62-72. https://doi.org/10.1016/j.coal.2012.04.005.

Malashkevych, D., Petlovanyi, M., Zubko, S. and Sai, K. (2022), **"**Research into the coal quality with a new selective mining technology of the waste rock accumulation in the mined-out area", *Min. Miner. Deposits*, **16**(4), 103-114. https://doi.org/10.33271/mining 16.04.103.

Oh, J. and Moon, T., Canbulat, I. and Moon, J.S. (2019), "Design of initial support required for excavation of underground cavern and shaft from numerical analysis", *Geomech. Eng.*, **17**(6), 573-581. https://doi.org/10.12989/gae.2019.17.6.573.

Rajwa, S., Janoszek, T. and Prusek, S. (2019), "Influence of canopy ratio of powered roof support on longwall working stability - A case study", *Int. J. Min. Sci. Tech*., **29**(4), 591-598. https://doi.org/10.1016/j.ijmst.2019.06.002.

Smoliński, A., Malashkevych, D., Petlovanyi, M., Rysbekov, K., Lozynskyi, V. and Sai, K. (2022), "Research into impact of leaving waste rocks in the mined-out space on the geomechanical state of the rock mass surrounding the longwall face", *Energies*, **15**(24), 9522. https://doi.org/10.3390/en15249522.

Song, Z.Q. (1988), Practical Mine Pressure Control, China University of Mining and Technology Press, Xuzhou, Jiangsu, China.

Tan, Y.L. (2021), Mine Pressure and Strata Control, Emergency Management Press, Beijing, China.

Vakili, A. and Hebblewhite, B.K. (2010), "A new cavability assessment criterion for Longwall Top Coal Caving", *Int. J. Rock Mech. Min.*, **47**(8), 1317-1329. https://doi.org/10.1016/j.ijrmms.2010.08.010.

Vu, T.T. (2022), "Solutions to prevent face spall and roof falling in fully mechanized longwall at underground mines, Vietnam", *Min. Miner. Deposits*, **16**(1), 127-134. https://doi.org/10.33271/mining16.01.127.

Wang, J.A., Yang, L. and Li, F. (2020), "Force chains in top coal caving mining", *Int. J. Rock Mech. Min*., **127**, 104218. https://doi.org/10.1016/j.ijrmms.2020.104218.

Wang, Q. and Su, X., Jin, Y., Sun, C., Yu, S., Zhao, W. and Feng, Y. (2023). "Experimental investigation of reservoir fluid interlayer crossflow through fracture during the drainage stage of coal measure gas well", *Nat. Resour. Res*., 16. https://doi.org/10.1007/s11053-023-10187-3

Wang, Y.J., Wang, Q., Tian, X.C., Wang, H. and Yang, J. (2022), "Stress and deformation evolution characteristics of gob-side entry retained by roof cutting and pressure relief", *Tunn. Undergr. Sp. Tech*., **123**, 104419. https://doi.org/10.1016/j.tust.2022.104419.

Xie, H.P, Chen, Z.H. and Wang, J.C. (1999), "Three-dimensional numerical analysis of deformation and failure during top coal caving", *Int. J. Rock Mech. Min. Geomech. Abstracts*, **36**(5), 651-658. https://doi.org/10.1016/S0148-9062(99)00027-3.

Yasitli, N.E. and Unver, B. (2005), "3D numerical modeling of longwall mining with top-coal caving", *Int. J. Rock Mech. Min.*, **42**(2), 219-235. https://doi.org/10.1016/j.ijrmms.2004.08.007

GC